Resistance in Steep Open Channels due to Randomly Distributed Macroroughness Elements at Large Froude Numbers

Suresh Kumar Thappeta[1]; S. Murty Bhallamudi[2]; Peter Fiener[3]; and Balaji Narasimhan[4]

Abstract: Energy loss in a steep open channel due to randomly spaced spherically shaped macroroughness elements such as boulders was investigated using a three-dimensional fluid dynamics solver. First, a relationship for energy loss at large Froude numbers due to a single boulder was derived as a function of flow rate, flow depth, and boulder diameter. Nondimensional energy loss increases with Froude number and decreases with the relative submergence. However, the exponents in the power law relationship are different for three different ranges of submergence ratio: <0.5, 0.5–1.0, and >1.0. The energy loss attributable to a cluster of boulders depends on cluster density, Froude number, and submergence ratio. For the same number of boulders, energy loss decreases as cluster density increases. However, variation in the pattern of boulder arrangement has only a marginal effect (<4%) when the submergence ratio is more than 0.5. The simple procedure proposed for estimating energy loss due to a cluster of randomly distributed boulders of equal size predicts energy loss within 10% accuracy.

Introduction

Understanding of flow behavior in steep open channels is essential for hydrologic and hydraulic modeling of mountain streams (Jordanova 2008; Modrick and Georgakakos 2014; Agostino and Michelini 2015), designing chute spill ways (Pagliara and Peruginelli 2000; Pagliara and Dazzini 2002) and fish passes (Cassan et al. 2014; Baki et al. 2014), and while studying the impact of development in mountainous areas in order to protect water resources, fisheries, biodiversity, recreation, and forestry (Thorne and Zevenbergen 1985). It is also needed for studying aggradation and degradation (Alonso et al. 2009), geomorphology (Chin 2003), and ecology (Yochum et al. 2012) of mountainous streams. Stream flows are a major determinant of physical habitat in streams and affect the distribution and abundance of stream biotic communities and influence the survival strategies of the aquatic organisms (Maloney et al. 2011). Assessment of energy loss constitutes one of the basic steps in such studies.

Energy loss in mountainous streams is strongly affected by the course, grain roughness due to cobbles and gravel on the bed (Hey 1979; Bathurst 1985), step pools (Comiti et al. 2007; Agostino and Michelini 2015), and macroroughness elements such as boulders

(Ferguson 2007; Jordanova 2008). Attempts have been earlier to empirically model flow resistance in mountainous streams in terms of Darcy-Weisbach friction factor or average flow velocity by considering several independent nondimensional hydraulic parameters such as relative submergence (ratio of flow depth to height of the roughness element), Froude number, Reynolds number, and concentration of roughness (Thompson and Campbell 1979; Bathurst et al. 1979, 1981; Hey 1979). Field data used for deriving the equations for friction factor in these studies represents completely submerged flow conditions and subcritical flows (Froude number 0.3–0.6). Proposed equations by Thompson and Campbell (1979) and Bathurst et al. (1979, 1981) were tested using field data collected from Boulder Creek in Colorado. It was found that velocities were overpredicted by as much as 30% (Thorne and Zevenbergen 1985).

Bathurst (1985) has modified an earlier model proposed by Hey (1979) for British lowland rivers, for application to mountain streams. This equation is valid for a relative submergence of 0.7–6.0 and Froude number of 0.27–1.17. Note that, in these works, relative submergence is defined as the ratio of the depth over the top of roughness elements to the size of the roughness elements. Similar studies were carried out by Aguirre-Pe and Fuentes (1990) for flows in open channel with low values of relative submergence. Soto and Madrid-Aris (1994) analyzed data on mountain streams and concluded that existing equations for resistance in mountainous streams were inadequate for characterizing large-scale roughness and intermediate-scale roughness elements. Romero et al (2010) used the data from five steep mountain rivers in Bolivia to assess the various empirical equations available for estimating Darcy-Weisbach friction factor. In all the previous studies, flow surface lies above the top of the roughness elements and thus these studies are applicable for completely submerged flow conditions.

Manning, Chezy, and Darcy-Weisbach equations, which are typically used for estimating energy losses in open-channel flows, do not adequately describe the energy loss generated by the macroroughness elements in mountain streams (Jordanova 2008; Ferguson 2010). Vortices that are generated in the wake and

[1]Ph.D. Scholar, Dept. of Civil Engineering, Indian Institute of Technology Madras, Chennai, Tamil Nadu 600036, India. E-mail: sthappeta@gmail.com

[2]Professor, Dept. of Civil Engineering, Indian Institute of Technology Madras, Chennai, Tamil Nadu 600036, India (corresponding author). E-mail: bsm@iitm.ac.in

[3]Professor, Institute for Geography, Univ. of Augsburg, Alter Postweg 118, 86159 Augsburg, Germany. E-mail: fiener@geo.uni-augsburg.de

[4]Professor, Dept. of Civil Engineering, Indian Institute of Technology Madras, Chennai, Tamil Nadu 600036, India. E-mail: nbalaji@iitm.ac.in

separated zones around macroroughness elements propagate downstream and dissipate after traveling some distance. They are one of the primary sources of energy loss in mountain streams. Classical equations for energy loss in open channels may not model this process adequately (Meier and Reichert 2005). Recently, Pagliara and Chiavaccini (2006) conducted an exhaustive experimental study on the flow resistance in rock chutes with protruding boulders. Presence of protruding boulders affected the channel geometry and modified the hydraulic resistance. For the tested range, Froude number, Reynolds number, and relative submergence did not have significant effect on the increased resistance. Ranges for experimental conditions were bed slope = 0.08–0.4; relative submergence = 0.5–10.5; Froude number = 0.8–2.9, and block density = 0.0–30%. Note that the number of experiments with relative submergence less than 1.0 were few in their experiments.

Baki et al. (2014) characterized resistance in open channels with spherical macroroughness elements on the bed. They considered uniform size boulders and structural arrangement as in rock-ramp type, nature-like fish pass. Also, their study was limited to the relative submergence ranging from 0.7 to 1.2. The flow resistance was expressed in terms of Chezy-type equation with a flow resistance coefficient, which depends on drag coefficient, number of boulders, and projected area. They did not consider the effect of Froude number on the drag coefficient. Cassan et al. (2014) proposed empirical equations for flow velocity in terms of ramp slope, block density, bed roughness, and flow depth in fish passes with cylindrical shape blocks. They discussed the importance of Froude number, besides the relative submergence, on the estimation of drag coefficient. In their experiments, the relative submergence varied from 0.5 to 1, and cylindrical elements were placed in a structured arrangement. Cassan and Laurens (2016) conducted experiments for submerged conditions. In a natural mountain stream, roughness elements are randomly distributed and are of nonuniform size. Although many experimental studies have been carried out in the recent past to understand the resistance in mountain streams induced by macroroughness elements, there is a need for more experiments, covering a wider range of flow and geometric conditions, for gaining further insight.

In recent past, computational fluid dynamics (CFD) models have been gaining popularity for studying complex free surface flow phenomenon such as flow structures in upland rivers during floods (Ma et al. 2002), flow around piers (Salaheldin et al. 2004), hydraulic jumps (Castillo et al. 2014; Xiang et al. 2014), flow around deflectors in fish habitats (Haltigin et al. 2007), and flow in vertical slot turning pools (Marriner et al. 2014), Shen and Diplas (2008) used three-dimensional (3D) CFD models for simulating complex flow conditions around an isolated hemisphere and a cluster of boulders under high and low flow conditions. Simulations were made for a relative submergence ranging from 0.78 to 4.6. The primary objective of this study was to demonstrate the effectiveness of 3D CFD models for simulating complex natural channel flows. No attempt was made to characterize energy loss induced by boulders in terms of flow and geometric parameters. Very recently, Baki et al. (2016) used a three-dimensional CFD model for simulating the flow characteristics in an open channel with spherical macroroughness elements. Numerical experiments were conducted to study the effect of channel slope, flow velocity, size of roughness elements, and spacing between elements on flow resistance. Data from these numerical experiments was used for deriving relationships for estimating water depth and velocity in a rock-ramp fish pass as a function of discharge and structure geometry. They also derived empirical equations for the drag coefficient as a function of submergence ratio. However, their study was limited to a total of 30 numerical experiments where the relative submergence varied from 0.7 to 1.2. Also, they did not consider the effect of randomly placed roughness elements and the effect of nonuniform size of elements.

This paper systematically characterizes the energy loss in a steep mountain channel due to macroroughness elements as a function of flow parameters (discharge and approaching flow depth), size of roughness elements, and number of roughness elements within a given area. The major objectives were (1) to test the capability of an existing 3D CFD model to simulate the spatial variation in velocity, the deformation of free surface and to estimate the energy loss in mountainous streams with submerged and emergent macroroughness elements; (2) to use the validated CFD model to derive and analyze energy losses in a series of simulation experiments; and (3) derive empirical equations for the energy loss induced by single, uniform clustered, and nonuniform clustered macroroughness elements as a function of flow and geometrical parameters.

Methodology

Three-Dimensional CFD Model

The existing CFD software package ANSYS-CFX was tested for its capability to simulate flow pattern around macroroughness elements in steep channels. This is a standard industrial software package and earlier versions of this package have been used to perform similar free surface flow studies (Shen and Diplas 2008; Baki et al. 2016). Therefore, only brief details about the software package are given in this paper and ANSYS-CFX can be referred for complete details. In ANSYS-CFX, a finite-volume approach (Evans et al. 1957) is used for numerically solving the three-dimensional Reynolds-averaged Navier-Stokes (RANS) equations, along with the standard k-ε model (Jones and Launder 1972) for turbulence closure. Earlier, Abdulla (2013) employed ANSYS-CFX with the standard k-ε turbulent model for simulating supercritical flows (Froude number 1.2–2.0) around bridge piers. Measured free surface along centerline, and vertical velocity profiles at different positions near the piers were compared using k-ε, RNG k-ε, and SST turbulent models and it was found that average percentage error between the models was insignificant, but computational time was the least for k-ε model. Among the different options available for tracking the free surface in the software, the option of volume of fluid (VOF) method (Hirt and Nichols 1981) was used. In this method, the volume fraction (VF) is defined as the volume of cell filled with water. A value of VF equal to one indicates that the cell is well below the water surface and a value of zero indicates that the cell is well above the water surface. Usually, a VF value of 0.5 is adopted for defining the water surface. In all the test cases, the mesh characteristic (Y+) was kept lower than 300 in order to satisfy dimensionless wall height criteria. Flow rate was specified as the inlet boundary condition and the flow velocity was uniform at the inlet.

Test Cases for Performance Evaluation of the Model

The performance of the ANSYS-CFX model was assessed using laboratory experimental data available in the literature (Jordanova 2008; Baki et al. 2014; Cassan et al. 2014). In Test Case 1 experimental data provided by Jordanova (2008) for flow in a 15 m long and 0.38 m wide rectangular flume, with a hemispherical roughness element (diameter 0.114 m) placed at the center of the flume at a distance of 4.5 m from the inlet was used [Fig. 1(a)]. The bed slope was 0.1136% and the flow rate was 0.005 m³/s. Velocities were measured using a two-dimensional Nortek Doppler velocimeter
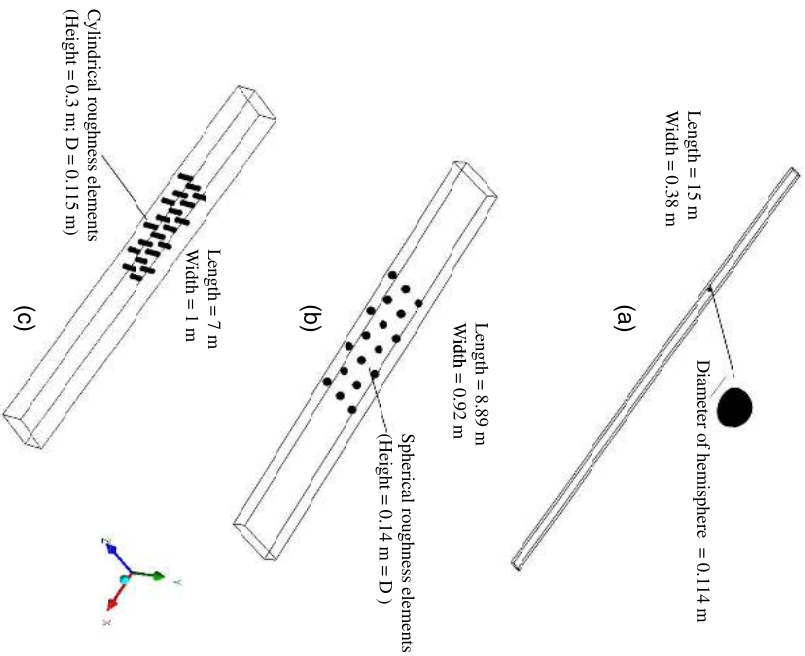
Fig. 1. Model domain for assessment of *ANSYS-CFX* package: (a) single hemispherical roughness element; (b) group of spherical roughness elements; (c) group of cylindrical roughness elements

(NDV) for 40 s at a frequency of 25 Hz, at different cross sections, at middepth (Jordanova 2008).

In Test Case 2, experimental data provided by Baki et al. (2014) for flow in an 8.89 m long and 0.92 m wide rectangular channel, with spherical roughness elements on the flume bed, as shown schematically in Fig. 1(b), were considered. The diameter of the spherical element was 0.14 m and the center to center distance between spheres was 0.375 m, arranged in a staggered pattern. In the first set of numerical experiments, the bed slope was 3% and the flow rate was varied as 0.04, 0.06, and 0.11 m³/s. In the second set of numerical experiments, the bed slope was 5% and the flow rate was varied as 0.06, 0.074, and 0.125 m³/s. The model domain considered in the present study was 3.5 m long, 0.92 m wide, and included 18 boulders. Diameter of each boulder is 14 cm, out of which 13 cm protruded above the bed.

In Test Case 3 experimental data provided by Cassan et al. (2014) for flow in a rectangular flume of length 7.0 m and width 1.0 m was used. The bed was smooth, and the cylindrical roughness elements were placed in a staggered pattern as shown schematically in Fig. 1(c). In their experiments, the bed slope varied between 0.01 and 0.09 and the flow rate varied from 0.01 to 0.09 m³/s. The center to center distance between the cylindrical elements was 0.333 m in both longitudinal and transverse directions. These experiments were conducted to mimic flow in a nature-like fish pass. Cassan et al. (2014) provided data for difference in water levels upstream and downstream of the cylindrical roughness elements for different Froude numbers. Also, based on the experimental data, they proposed an empirical relationship between the flow rate and discharge for different bed slopes and macroroughness characteristics.

Boundary Conditions and Discretization

In the numerical simulations, boundary conditions were specified as follows. The top of the domain was located much above the expected free surface, and therefore atmospheric pressure condition was specified at this boundary. Flow rate was specified at the inflow or the left boundary. A turbulent intensity of 5% was applied to specify turbulent kinetic energy and dissipation rate of fluid (Baki et al. 2016) at the inlet boundary. At the outflow or the right boundary, pressure, as obtained using the hydrostatic condition for the specified depth, was specified as the boundary condition. A no-slip condition was applied at the bottom boundary, side wall boundaries, and all the solid boundaries of submerged parts of roughness elements. Surface roughness in *ANSYS-CFX* can be given as equivalent sand grain roughness. Manning's roughness value was converted to equivalent sand grain roughness height using the equation proposed by Marriott and Jayaratne (2010). Manning's roughness value was 0.012 for wooden cylinders used by Cassan et al. (2014) and the bottom and the sides were treated as smooth. In the simulation of experiments carried out by Baki et al. (2016), the equivalent sand grain roughness height value for both the floor and the sides was 0.8 mm. In the simulations for experiments by Jordanova (2008), the roughness heights for floor and the roughness elements were 0.8 mm and 0.97 mm, respectively. Option of high resolution scheme was chosen for discretizing the advection terms. A residual of 0.0001 was specified as the convergence criterion. All simulations were carried out for steady state conditions and the solution converged within 1,000 iterations.

An unstructured tetrahedral mesh was used in the solution domain. Inflation was adopted for refining the mesh near the bottom boundary and face sizing was adopted for all roughness elements using a mesh size of 0.6 mm. The numerical mesh, with a variable size, was created using the ICEM CFD subroutine in *ANSYS-CFX*. Similar meshes were used in other cases. Grid sensitivity tests were carried out for experiments conducted by Jordanova (2008) using four mesh sizes of 17.5, 13.5, 10.0, and 7.5 mm. In these runs, the total number of nodes varied from 577,798 to 2,531,562, while the total number of elements varied from 2,531,562 to 6,504,731. Results from the previous numerical runs for streamwise velocity profiles at $x = 3.5$ m and depth = 0.022 m above the bed are compared in Fig. 2. It is shown from these grid sensitivity tests that a mesh size of 10.0 mm was satisfactory because this size gave grid convergent results. Difference in results obtained using this mesh size and a finer mesh size of 7.5 mm was insignificant as illustrated in Fig. 2.
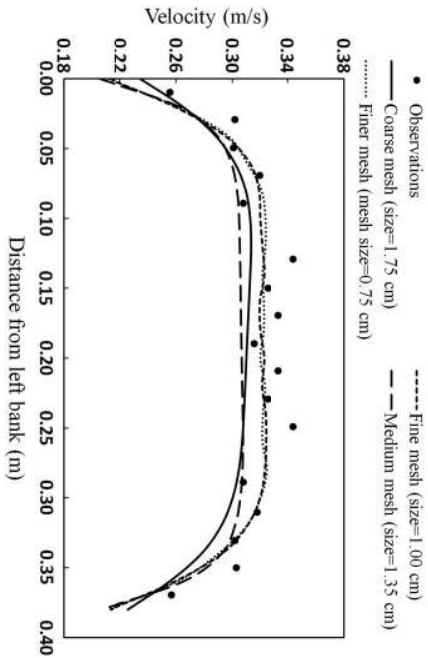
Model Testing

Root mean square error (RMSE), bias, and coefficient of efficiency (E) were used for assessing the agreement between observed and simulated data

$$\text{RMSE} = \sqrt{\frac{1}{n}\sum_{i=1}^{n}(O_i - S_i)^2} \qquad (1)$$

$$E = 1 - \frac{\sum_{i=1}^{n}(S_i - O_i)^2}{\sum_{i=1}^{n}(O_i - \bar{O})^2} \qquad (2)$$

$$\text{Bias} = \frac{\sum_{i=1}^{n}(O_i - S_i)}{n} \qquad (3)$$

Velocity (m/s)

• Observations
—— Coarse mesh (size=1.75 cm)
······ Finer mesh (mesh size=0.75 cm)
---- Fine mesh (size=1.00 cm)
— — Medium mesh (size=1.35 cm)

Distance from left bank (m)

Fig. 2. Mesh sensitivity analysis; simulated streamwise velocities at $x = 3.50$ m and midheight

where O_i and S_i are observed data and simulated results, respectively. Over bar indicates the average of all the observed values and n is the number of data points.

Numerical Experiments

Following the validation of *ANSYS-CFX* against the literature data, the model was used to conduct extensive numerical experiments to gain insight into energy loss induced by large roughness elements in steeply sloped open channels, such as those found in mountainous areas. Numerical experiments were limited to supercritical flow conditions and spherical shaped roughness elements. Numerical experiments were carried out for (1) an isolated or single element in a long channel (51 runs), (2) a cluster of uniformly sized, randomly placed roughness elements (60 runs); and (3) a cluster of nonuniformly, randomly placed sized roughness elements as in Fig. 3 (12 runs). Data for these numerical experiments is provided in Tables S1–S3 in Supplemental Data. In all these numerical experiments, the flow rate was varied between 0.05 and 0.45 m³/s and the diameter of spherical boulder was varied between 3.6 and 49.8 cm. The bed slope, S_0, and sand grain roughness, k_s, were kept constant and were equal to 5% and 8.54×10^{-5} m, respectively. In the experiments for cluster of boulders, the maximum

number of boulders was as high as 30 and they were placed randomly. The area enclosing the cluster (Fig. 3) of boulders varied from 0.025 to 1.24 m².

In each numerical experiment, three-dimensional turbulent flow conditions were simulated using the *ANSYS-CFX* for specified (1) flow rate at the inflow section, (2) flow depth at the outflow section, (3) bed roughness (equivalent sand grain roughness height, k_s), and (4) locations of roughness elements and corresponding sizes (diameters, D). Boundary conditions were specified as described earlier. The numerical simulation gave the complete three-dimensional flow structure, which was used to determine the total energy TE_u at a section upstream (Section u), and total energy TE_d at a section downstream (Section d) of the roughness elements, as shown in Fig. 3. The total energy loss between Sections u and d, ΔTE was the difference between TE_u and TE_d. This consists of friction loss due to bed and the form loss due to roughness elements. A numerical experiment was carried out in parallel for exactly the same flow rate, bed slope, and channel roughness, but without the presence of large roughness elements. These numerical simulations were used to estimate the energy loss between the Sections u and d due to bed friction, ΔE_{bed}. Energy loss between Sections u and d due to roughness elements, ΔE, was then estimated as the difference between ΔTE and ΔE_{bed}. For example, in Run 14 ΔTE and ΔE_{bed} were 0.077 and 0.044 m. Therefore, ΔE was estimated as 0.033 m.
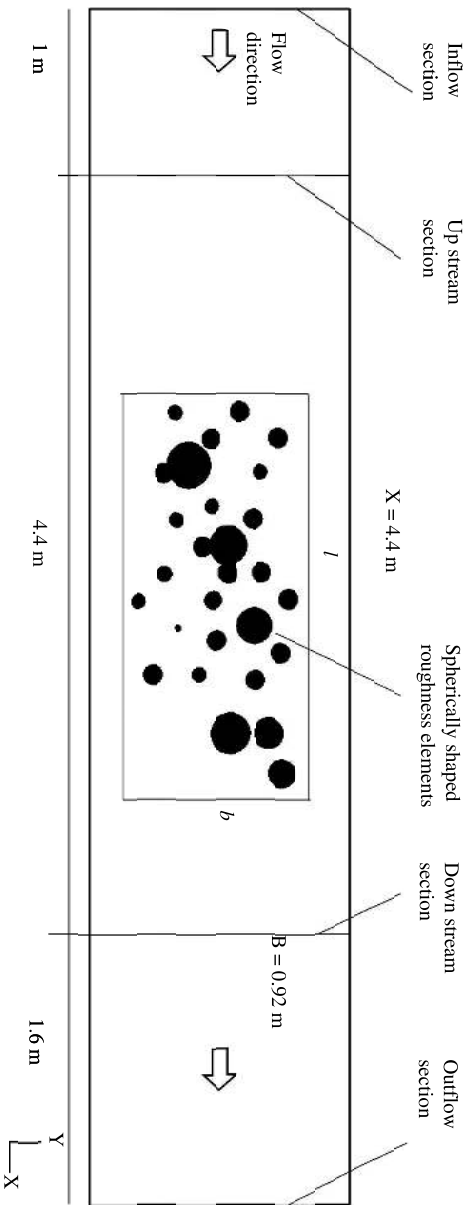
Empirical Equations for Energy Loss

Energy loss due to a single isolated spherical boulder can be written as a function of several parameters as shown subsequently

$$\Delta E = F[V_u, H_u, D, L_u, \rho, g, \mu] \qquad (4)$$

where ΔE = energy loss due to the boulder; L_u = distance between upstream section and boulder location; ρ = density of water; μ = dynamic viscosity; V_u = average velocity at upstream section; H_u = average flow depth at upstream section; D = diameter of sphere; and g = gravitational acceleration. Application of dimensional analysis yields the following functional relationship between the nondimensional parameters

$$\Delta E_{single}^* = \left[\frac{\Delta E}{L_u}\right]_{single} = F\left[\frac{4\rho V_u H_u}{\mu}, \frac{H_u}{D}, \frac{V_u}{\sqrt{gH_u}}, \frac{H_u}{L_u}\right] \qquad (5)$$

Inflow section   Up stream section   X = 4.4 m   Spherically shaped roughness elements   Down stream section   Outflow section

Flow direction

l b B = 0.92 m

1 m   4.4 m   1.6 m

Y   X

Fig. 3. Characteristic dimensions

where $4\rho V_u H_u/\mu = R_u$ = Reynolds number at the upstream section; H_u/D = relative submergence; and $V_u/\sqrt{gH_u} = F_u$ = Froude number at the upstream section.

It is proposed to estimate the energy loss due to a cluster of uniformly sized boulders based on the energy loss due to a single boulder and the number of boulders as given subsequently

$$\Delta E_{\text{cluster}} = I_f [N] [\Delta E_{\text{single}}] \qquad (6)$$

where $\Delta E_{\text{cluster}}$ = energy loss due to cluster; ΔE_{single} = energy loss if only one roughness element is present; N = number of roughness elements; and I_f = interaction factor that accounts for interaction between different roughness elements. At the outset, it is obvious that the energy loss should depend on the cluster density (Pagliara and Chiavaccini 2006; Cassan et al. 2014; Baki et al. 2016). Preliminary numerical experiments indicated that while the I_f depends on the cluster density, it is not significantly affected by the way roughness elements are spatially distributed. In this paper, cluster density is defined as the ratio between area occupied by N number of boulders and the encompassed cluster area ($l.b$) as shown in Fig. 3

$$\text{Cluster Density} = \lambda = \frac{N\frac{\pi}{4}D^2}{l.b} \qquad (7)$$

It is also shown that the interaction should depend on the flow and other geometrical parameters. Therefore, following functional relationship is proposed for the interaction factor, I_f

$$I_f = f\left[F_u, \frac{H_u}{D}, \frac{H_u}{L_u}, \lambda\right] \qquad (8)$$

In nature, all the boulders in a cluster may not be of the same size, as schematically shown in Fig. 3. An attempt is made in this study to estimate the energy loss in such cases, based on the concept of effective boulder size, D_{eff}. It is assumed that the energy loss would be equal to the energy loss due to a cluster of same number of boulders, each having a diameter equal to D_{eff}. Effective diameter is defined as given subsequently

$$D_{\text{eff}} = \sqrt{\frac{D_1^2 + D_2^2 + \cdots + D_N^2}{N}} \qquad (9)$$

where $D_1, D_2, D_3, \ldots, D_N$ = individual diameters of boulders. Rest of the procedure for estimating the energy loss is the same as described earlier for a cluster of uniformly sized boulders, as summarized as follows:

- Determine D_{eff} using Eq. (9);
- Determine the energy loss due to a single boulder based on the previous D_{eff} value and the other geometric and flow conditions (Q, H_u, and L_u) using Eq. (5);
- Determine the interaction factor I_f based on the density λ, the geometric parameters and the flow parameters (F_u, H_u/L_u, and H_u/D_{eff}) using Eq. (8); and
- Determine the energy loss due to the cluster using Eq. (6)

Results and Discussions

Evaluation of the ANSYS-CFX Model

The performance of the ANSYS-CFX model was evaluated using three test cases as mentioned earlier. Simulated velocity profiles at different cross sections for Test Case 1 are compared with the measured data (Jordanova 2008) in Fig. 4. Velocity measurements were taken at middle of the flow depth for different cross sections.

It can be observed that the simulated velocity profiles matched well with the observed velocity profiles. The RMSE, bias, and E values for the Test Case 1 are in the range 0.009 to 0.029 m/s, −0.0045 to −0.0093 m/s, and 0.48 to 0.892, respectively. Appreciable error occurred only for the cross section at $x = 4.4$ m. There is a discrepancy of 10% in the prediction of maximum velocity. However the nature of velocity distribution is simulated well.

The overall agreement between the observed and simulated vertical variation in streamwise velocity along the central vertical plane in Test Case 2 (Baki et al. 2016) is shown in Fig. 5. Velocity profiles are shown for two runs. In results shown in Fig. 5(a), the bed slope was 5% whereas it was 3% in results shown in Fig. 5(b). In both the cases, flow rate was 0.06 m³/s. The RMSE, bias, and E values in the wake zone for 5 and 3% bed slopes were 0.049 m/s, −0.015 m/s, 0.92, and 0.098 m/s, −0.07 m/s, 0.95, respectively. Intensive turbulence in the wake region caused the occurrence of maximum difference between the observed and simulated streamwise velocities in this region. Similar results were reported by Baki et al. (2016). Comparison between numerical and observed results in their study also showed an RMSE value of 0.069 m/s for 5% slope and 0.0587 m/s for 3%. The vortices and reverse flow are created in the wake region by the adverse pressure gradient and the recirculation. This extends to several boulder diameters on the downstream side.

Based on their experimental data, Baki et al. (2014) proposed the following empirical equation for estimating depth averaged velocity at any section within the fully developed region

$$u_{\text{avg}} = C^* \sqrt{S R_v} \qquad (10a)$$

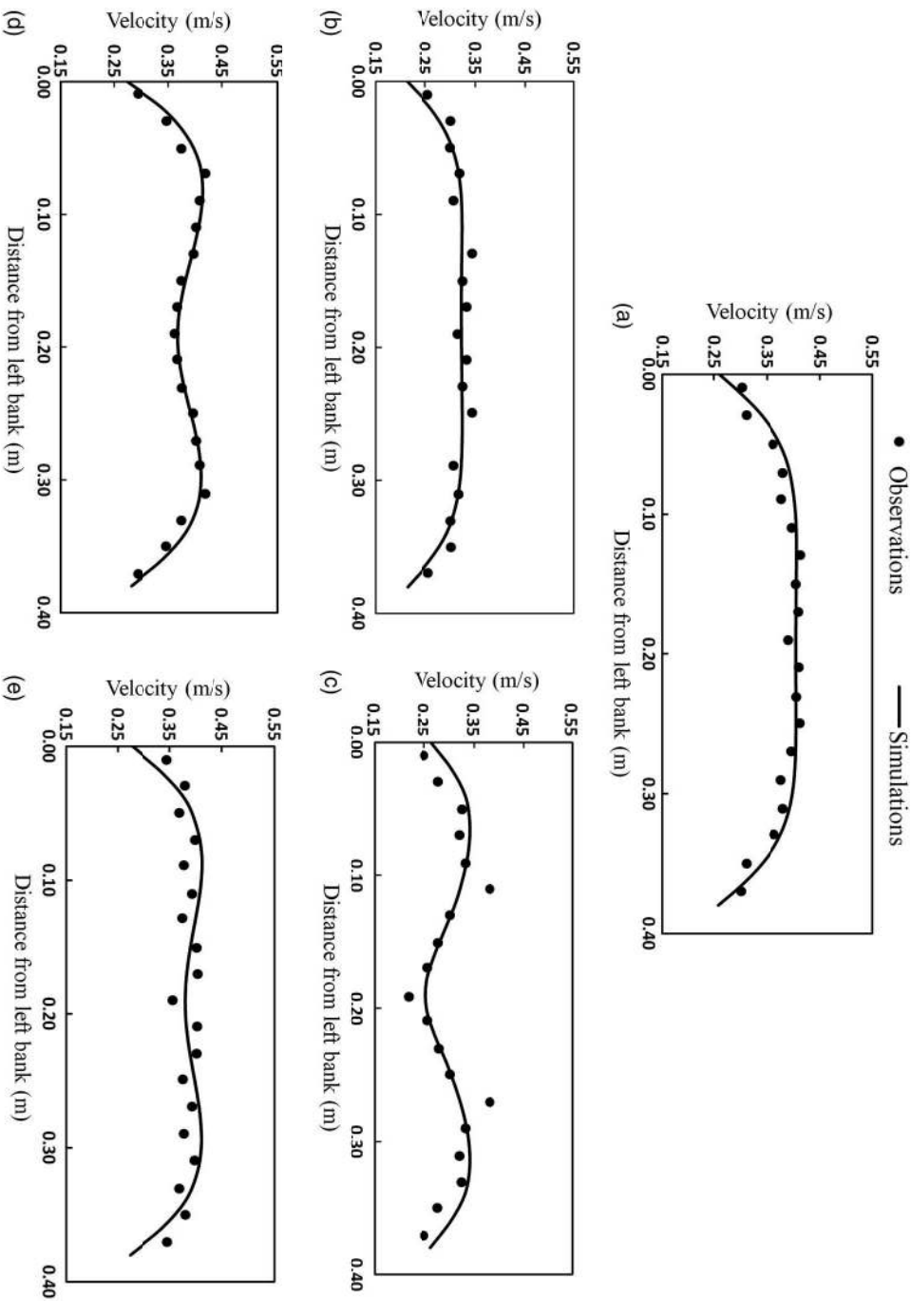$$C^* = \sqrt{\frac{2g}{C_D N A_p}} \qquad (10b)$$

$$R_v = H\left[1 - \frac{2}{3 I^* \lambda}\right] \qquad (10c)$$

$$C_D = 1.787\left(\frac{H}{D}\right)^{-2.16} \qquad (10d)$$

where S = slope; C^* = flow resistant coefficient; R_v = volumetric hydraulic radius; N = number of boulders; A_p = projected cross-sectional area of each boulder; λ = fraction of bed area occupied by boulders; $I^* = D/H$; D = diameter of boulder; H = average water depth along center line; and C_D = drag coefficient. Values for C^* and R_v are calculated using Eqs. (10b) and (10c); and C_D is estimated using Eq. (10c) (Baki et al. 2016).

In the present study, for any numerical experiment with specified values for (1) flow rate at the inflow of the domain; (2) N, and λ; (3) diameter of boulders; and (4) bed slope, S, simulated values of H were first used to determine C^* and R_v. Subsequently, Eq. (10) was used to determine u_{avg} and then the unit flow rate, q_{com}. This value of q_{com} is compared with q_{spec} at the inlet for several numerical runs in Fig. 6. It can be observed from Fig. 6 that the numerical results satisfactorily match with the experimental data for flow resistance in Baki et al. (2014). RMSE, bias, and E values for estimated flow rate are 0.0067 m²/s, 0.0026 m²/s and 0.954, respectively.

In Test Case 3, numerical results were verified by comparing the simulated deformation of free surface around a roughness element with empirical equations [Eqs. (11a) and (11b)] proposed by Cassan et al. (2014) based on experimental data

(a)

Velocity (m/s)

0.55 0.45 0.35 0.25 0.15

0.00 0.10 0.20 0.30 0.40
Distance from left bank (m)

● Observations   — Simulations

(b)

Velocity (m/s)

0.55 0.45 0.35 0.25 0.15

0.00 0.10 0.20 0.30 0.40
Distance from left bank (m)

(c)

Velocity (m/s)

0.55 0.45 0.35 0.25 0.15

0.00 0.10 0.20 0.30 0.40
Distance from left bank (m)

(d)

Velocity (m/s)

0.55 0.45 0.35 0.25 0.15

0.00 0.10 0.20 0.30 0.40
Distance from left bank (m)

(e)

Velocity (m/s)

0.55 0.45 0.35 0.25 0.15

0.00 0.10 0.20 0.30 0.40
Distance from left bank (m)

Fig. 4. Observed and simulated velocity profiles for Test Case 1: (a) uniform flow without the sphere; (b) at $x = 3.5$ m; (c) at $x = 4.4$ m; (d) at $x = 5.5$ m; (e) at $x = 6.5$ m

where h = average of water depth on upstream and downstream sides of block; $\mathbf{F}$ = Froude number based on velocity between blocks; and Δh = difference between flow depths on the upstream side of the cylinder and downstream of the cylinders. Eq. (11b) is for subcritical flows and Eq. (11a) is for supercritical flows. Fig. 7(a) shows the scatter plot between $\Delta h/h$ and $\mathbf{F}$ for both numerical simulations and the experimentally observed data. The equation proposed by Cassan et al. (2014) [Eq. (11)] is also plotted in this figure. It can be observed from Fig. 7(a) that there is a good agreement between the numerical results and the proposed empirical equation. Numerical results are also verified using the empirical equation proposed by Cassan et al. (2014) for estimating flow rate, if flow depth, bed slope and information about roughness elements are provided, using the following equation:

$$\frac{\Delta h}{h} = \frac{F^2}{2} \qquad (11a)$$

$$\frac{\Delta h}{h} = \frac{F^{2/3}}{2} \qquad (11b)$$

$$q_* = \frac{q}{\sqrt{g}D^{3/2}} = h_* \left(1 - \sqrt{\frac{\sqrt{a_y C}}{a_x}}\right) \sqrt{\frac{2S(1 - \sigma C)}{C_d C(1+N)}} \qquad (12)$$

where q_* = nondimensional flow; q = flow rate per unit width; $h_* = h/D$; D = cylinder diameter; a_x, a_y = center to center distance between cylinders in longitudinal and transverse directions; C = roughness concentration = $D^2/(a_x a_y)$; S = bed slope; C_d = drag coefficient; $N = \alpha\, c_f/c_d\, Ch_*$ = ratio between bed friction force and drag friction force; and σ = ratio between block area and D^2.

Eq. (12) is a semiempirical equation and was proposed by Cassan et al. (2014) based on their experimental data. In the present numerical runs, q is specified as input, and h is obtained as output, and then Eq. (12) is used to determine q_{computed}. Numerically estimated values of q, i.e., q_{computed} are compared with the specified values of q in Fig. 7(b). Once again, it can be observed that the numerically estimated discharges match well with the specified values. The RMSE, bias, and E values for computed flow rate using Cassan et al. (2014) model [Eq. (12)] and flow rate specified at inlet are 0.00487 m²/s, −0.0024 m²/s, and 0.94, respectively, and all points are lying within 5% error.
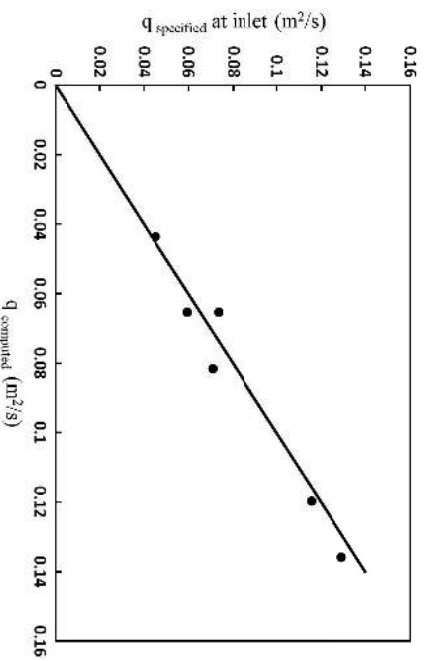
It can be concluded from the previous discussion that *ANSYS-CFX* can be used for successfully simulating the complex flows in open channels with macroroughness elements. Although there is some error in the magnitude of velocity in immediate vicinity of the roughness element, the *ANSYS-CFX* is able to simulate the overall flow structure and the simulations are satisfactory for the purpose of estimating the energy loss.
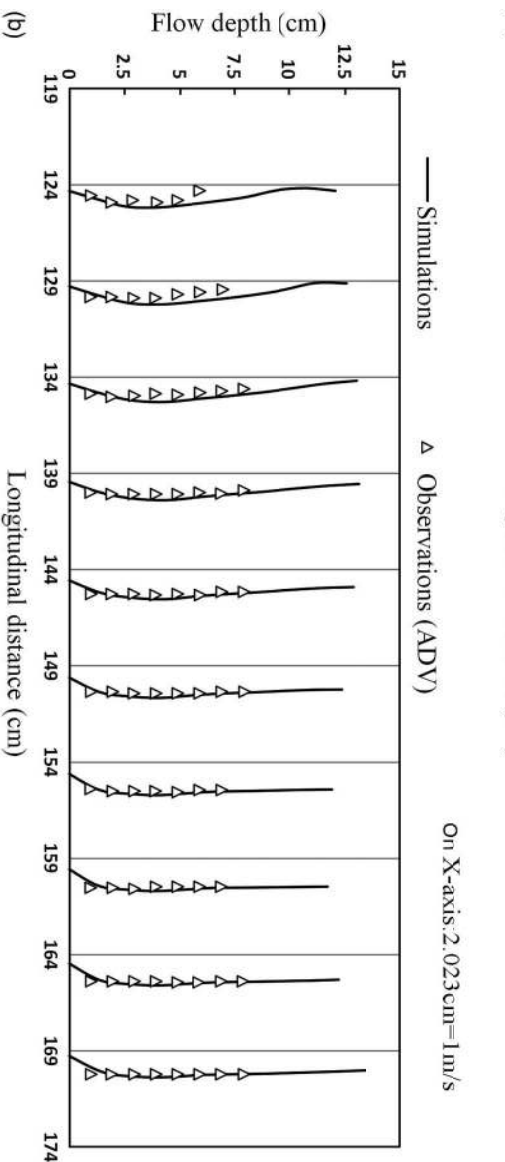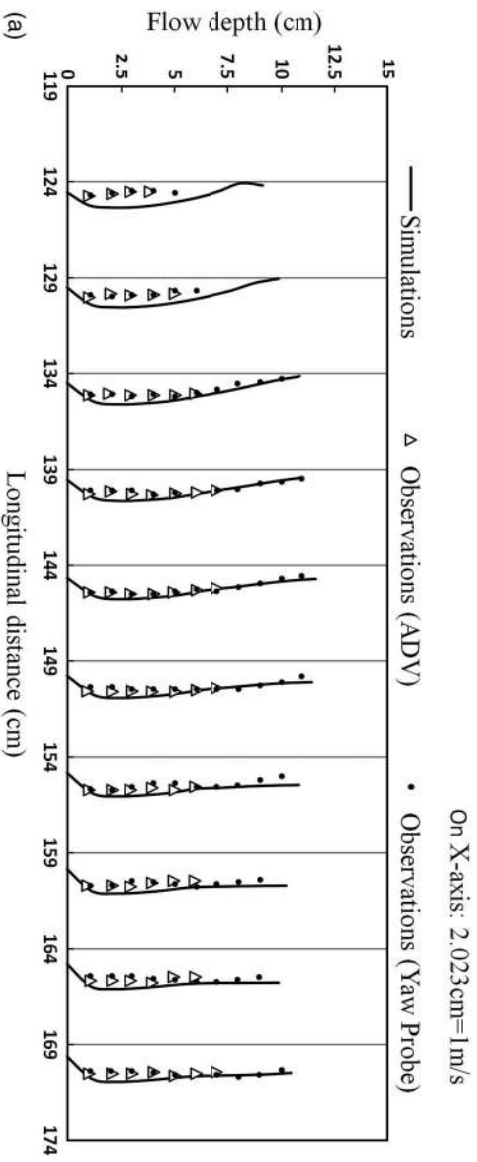
Energy Loss due to a Single Boulder

In this section, the energy loss induced by a single boulder is presented. Fig. 8 shows the velocity variation along the central vertical plane for three different relative submergence (H_u/D) values of 0.33, 0.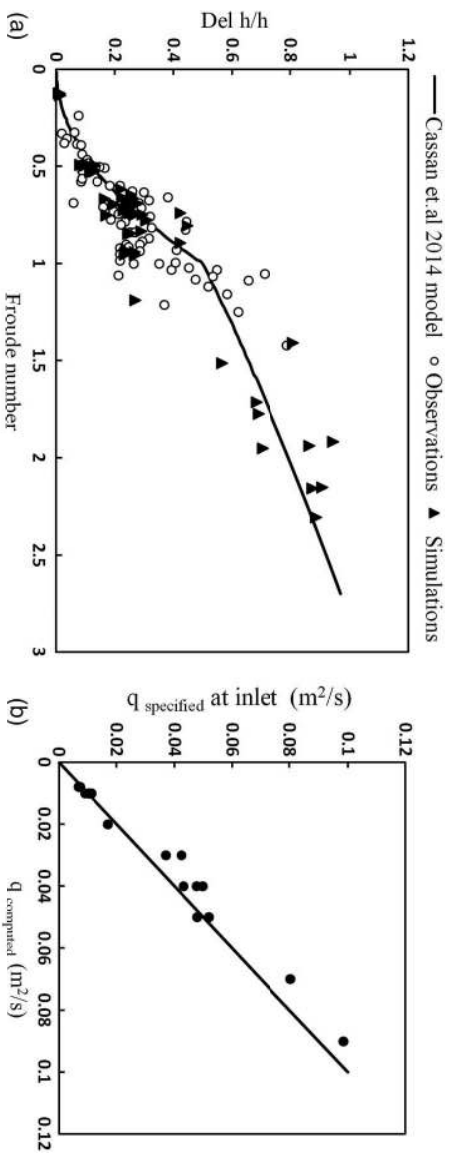84, and 1.49. In this paper, H_u is the flow depth at the upstream Section u, and D is the diameter of the boulder. In these three numerical runs, the flow rate was 0.2 m³/s, bed slope was 5%, and H_u was 0.116 m. Only the diameter of the boulder was varied. It is shown in Fig. 8 that the flow pattern varied significantly as the relative submergence increased. In all the three cases, the water level increased ahead of the boulder and then decreased in the wake region. These modeling results are consistent with the observations made by previous researchers (Baki et al. 2014; Cassan et al. 2014). The change in the water level is most significant when relative submergence is 0.33. The rise in the water level was not sufficient for water to flow over the boulder. However, when the relative submergence was 0.84, the rise in water level in front of the boulder was sufficient to make the water to flow over the boulder. The water level decreased on the downstream side and it was below the top of boulder. When the submergence ratio was 1.49, although there was a change in the water level due to the boulder, this change was not as high as when the H_u/D ratio was less than 1. Correspondingly, the spatial variation in velocity, on both upstream and downstream sides of the boulder, was also very different, as shown in Fig. 8. The effect of boulder on the flow persisted for longer lengths on the downstream side, as the H_u/D value was decreased.

Computations for ΔE indicated that the energy loss due to boulder increased as the H_u/D decreased. This is consistent with conclusions from earlier studies (Bathurst et al. 1981; Bathurst 1985; Baki et al. 2016). In the present case, ΔE was equal to

Fig. 5. Velocity profile comparison: (a) 0.06 m³/s flow rate and 5% bed slope; (b) 0.06 m³/s flow rate and 3% bed slope

Fig. 6. Validation using flow resistance model proposed by Baki et al. (2014)

Fig. 7. Measured and simulated: (a) free surface deformation with Froude number; (b) validation Cassan Model [Eq. (12)]

Water.Velocity

0.0 0.2 0.4 0.6 0.8 1.0 1.2 1.4 1.6 1.8 2.0 2.2 2.4 2.6 2.8

[m s⁻¹]
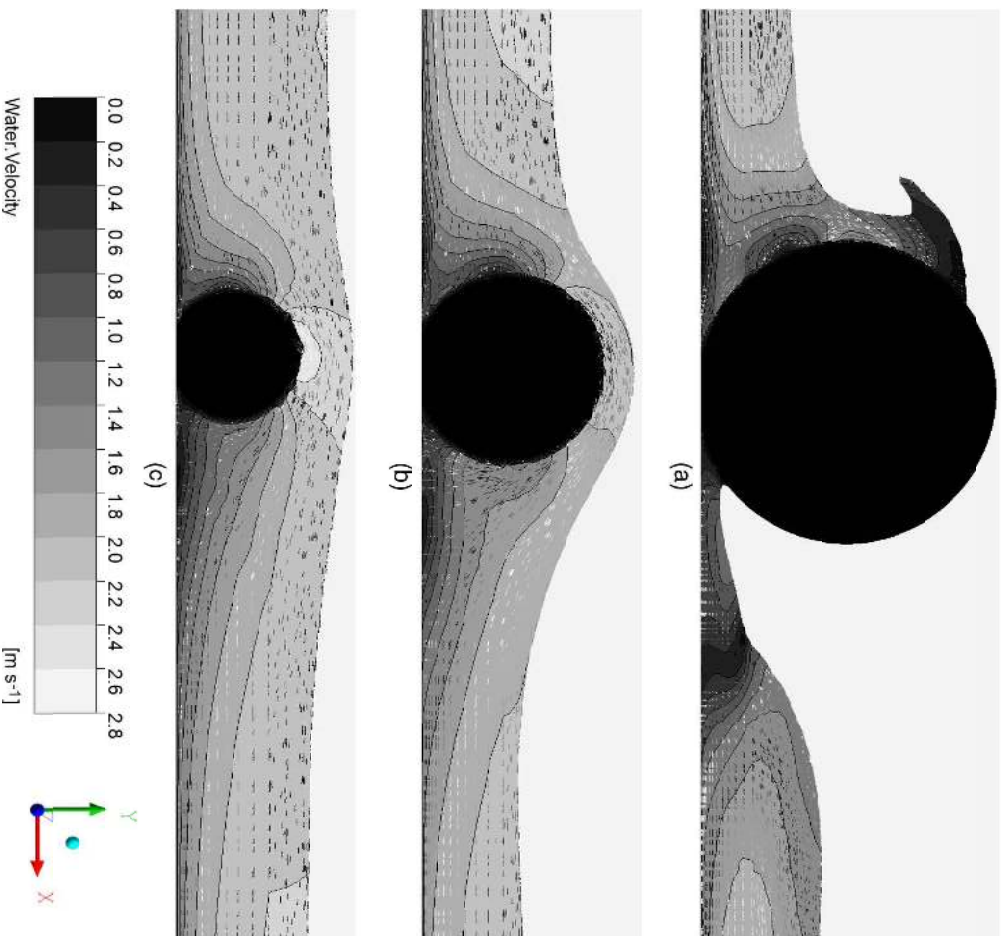
Fig. 8. Spatial variation of velocity on the central vertical plane for different cases of relative submergence (other conditions remain same): (a) Run 5; (b) Run 29; (c) Run 48

63 mm when H_u/D was 0.33, and it was only 9 mm when H_u/D was 1.49. In an earlier study, Oertel et al. (2011) defined three different flow regimes based on three ranges for relative submergence: $0.0 < H_u/D < 1.0$; $1.0 < H_u/D < 2.0$, and $H_u/D > 2.0$. In the present study, the authors delineated the three flow regimes

corresponding to H_u/D ratio as: $0.0 < H_u/D < 0.5$; $0.5 < H_u/D < 1.0$; and $H_u/D > 1.0$.

Numerical experimentation indicated that the energy loss attributable to the boulder depends on the location of the boulder from the upstream section, L_u, when all the other flow conditions and the
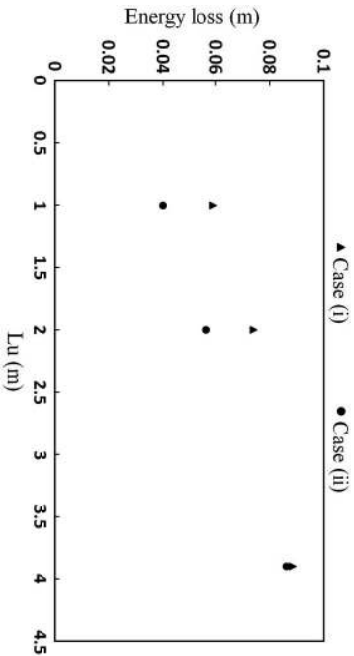
size of the boulder remain constant. Numerical experiments were carried out for a flow rate, $Q = 0.45$ m³/s; Froude number at upstream section, $F_u = 2.76$; $H_u = 0.142$ m; and $D = 0.18$ m. Numerical runs were made for three different L_u values of 1.0, 2.0, and 4.9 m and the results for ΔE are presented in Fig. 9 [Case (i)]. It is shown from Fig. 9 that the energy loss due to boulder, ΔE increased as the distance from the upstream section increased, for the above flow conditions. This dependence of ΔE on L_u arises because the flow pattern in the wake region depends on the flow conditions just ahead of the boulder. Given the same flow conditions at the upstream section (Section u), flow conditions just ahead of the boulder depend on how far the boulder is located from the Section u because of channel bed friction losses. Similar results [Fig. 9, Case (ii)] were obtained for the case of flow rate, $Q = 0.10$ m³/s, Froude number at upstream section, $F_u = 1.77$, $H_u = 0.068$ m, and $D = 0.354$ m.

Preliminary experimentation has shown that the energy loss is not a function of Reynolds number when the flow is highly turbulent. Similar observations were made by Bathurst (1985) and Ferro (2003) for mountain streams with gravel beds and rock chutes. Therefore, Froude number, relative submergence, and ratio between average flow depth at upstream section and the distance to boulder were considered as independent variables and nondimensional energy loss was considered as dependent variable. A total of 51 simulations were made with the following ranges for independent parameters: $1.4 < F_u < 2.8$; $0.2 < (H_u/D) < 2.4$; and $0.017 < (H_u/L_u) < 0.15$. The nondimensional energy loss due to the boulder, ΔE^*_{single}, is fitted as a function of the previous three nondimensional parameters using a power function. Among the many forms of equations tried, power law fitted the experimental data best. In an earlier study, Bathurst (2002) also concluded that a power law describes the flow resistance better than semilogarithmic law. Baki et al. (2014) also used a power law to estimate the drag coefficient, which in turn was used to describe the resistance relationship for a cluster of boulders. In the present study, the equation for energy loss was fitted independently for the three ranges of relative submergence as follows:

$$\left(\Delta E/L_u\right) = 0.054 \times F_u^{2.30}\left(\frac{H_u}{D}\right)^{-0.46}\left(\frac{H_u}{L_u}\right)^{0.845}$$
$$\text{for } 0.2 < \frac{H_u}{D} < 0.5 \tag{13a}$$

$$\left(\Delta E/L_u\right) = 0.0014 \times F_u^{2.20}\left(\frac{H_u}{D}\right)^{-1.77}\left(\frac{H_u}{L_u}\right)^{0.64}$$
$$\text{for } 0.5 < \frac{H_u}{D} < 1.0 \tag{13b}$$

$$\left(\Delta E/L_u\right) = 0.062 \times F_u^{1.42}\left(\frac{H_u}{D}\right)^{-1.61}\left(\frac{H_u}{L_u}\right)^{0.88}$$
$$\text{for } 1.0 < \frac{H_u}{D} < 2.4 \tag{13c}$$
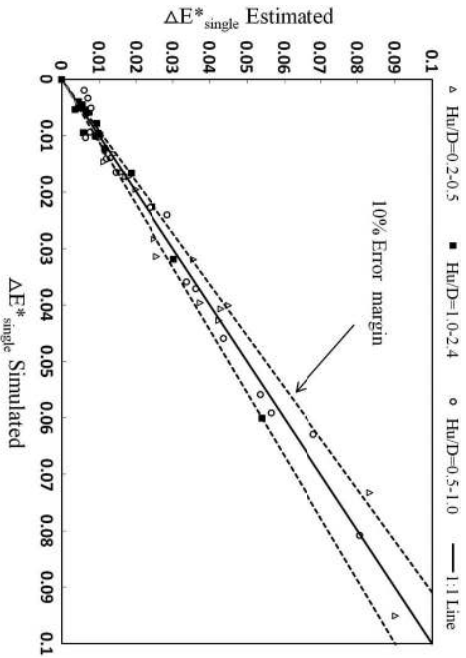

Fig. 9. Effect of boulder location on energy loss

Note that the energy loss due to the single boulder increased as the Froude number increased and it decreased as the relative submergence increased. The dependence of energy loss on relative submergence is similar to the dependence of drag coefficient, C_D on H_u/D, as obtained by Baki et al. (2016) in their study on rock-ramp fish pass. The prefactor first decreases (for $1 > H_u/D > 0.5$) and then increases (for $H_u/D > 1$) as the relative submergence increases. Also, there is a significant difference in the exponent of F_u as the relative submergence increases. This is because of significant difference in flow pattern (velocity variation, free surface elevation, and flow separation) downstream of the roughness element as the complete submergence occurs. The flow pattern affects the drag coefficient and thus the energy loss. For example, flow pattern and free surface profiles for Runs 5, 29, and 48 are shown in Fig. 8. The upstream Froude number and flow depth are the same in all these three runs and the only difference is the relative submergence owing to the size of the sphere. As discussed earlier, the effect of submergence ratio on the flow structure is clearly discernible from this figure.

Note that for the same approach flow conditions i.e. F_u and H_u/D, the energy loss increases as the distance to boulder, L_u, increases in all cases. Strictly speaking, bed slope and bed roughness should not affect the form loss due to flow around macroroughness elements. Experimental study of Pagliara and Chiavaccini (2006) indicated that bed slope does not effect the energy loss due to macroroughness elements for slopes less than 30%. The dependence of ΔE on L_u in the present study is because of the nonuniform flow conditions between upstream Section u and the location of the roughness element. The particular approach for energy loss characterization as the loss between an upstream Section u and a downstream Section d was adopted keeping in mind the discretization procedures (e.g., standard step method) usually adopted in open channel flow computations. This necessitated consideration of L_u as a dependent variable. However, the difference in flow conditions between Section u and a section just upstream of roughness element depend not only on L_u but also on the slope of the channel and the bed roughness. In all the numerical experiments carried out in this study, the bed slope and the channel roughness were kept constant at 5% and 8.54×10^{-5} m. This is clearly a limitation of the model at the present stage of development. Further numerical experiments need to be carried out and the prefactor in the power law model should be expressed as a function of the bed slope and the channel roughness. In such a procedure, the exponents of the existing nondimensional parameters in the power law model would not change. Further investigations will be undertaken in future to address this issue.

Energy loss values obtained using the fitted Eq. (13) (estimated) are compared with the energy loss values determined based on the three-dimensional numerical simulations (pseudoexperimental) for all the 51 simulations in Fig. 10. It is shown in Fig. 10 that most of the data points are within 10% error margin.

Energy Loss due to a Cluster of Boulders

In this section, the authors present the energy loss induced by a cluster of boulders in an open channel. In most of the previous studies (Jordanova 2008; Baki et al. 2014, 2016; Cassan et al. 2014), the pattern of placement of boulders or roughness elements was regular. In the present study, the authors consider random placement of
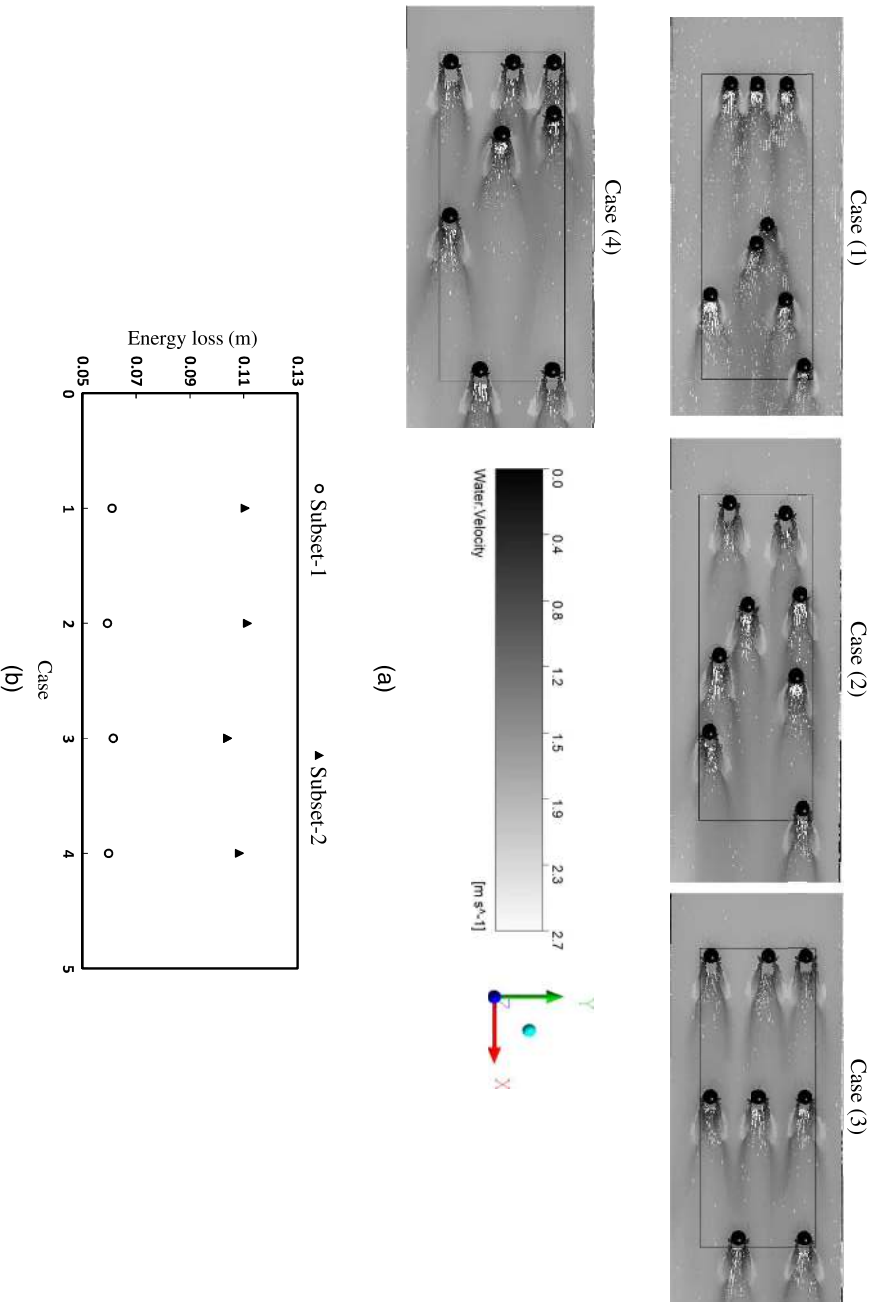
Fig. 11. Variation in energy loss for different spatial distributions, all other parameters remaining the same: (a) schematic for different spatial distributions; (b) energy loss variation


(a)

Case (1)

Case (2)

Case (3)

Case (4)

Water:Velocity

[m s^-1]

(b)

Energy loss (m)

Case

○ Subset-1   ▲ Subset-2

Fig. 10. Comparison of empirically estimated and numerically simulated energy losses

ΔE*single Estimated

ΔE*single Simulated

10% Error margin

△ Hu/D=0.2-0.5   ■ Hu/D=1.0-2.4   ○ Hu/D=0.5-1.0   —— 1:1 Line

a number of boulders in a given area, and study how the energy loss due to this cluster of boulders depends on the flow conditions and the interaction between boulders (Fig. 3).

First, numerical experiments were carried out to study the effect of random spatial distribution of uniform sized spherical roughness elements (Fig. 11) on the energy loss. In the first subset of experiments, $F_u = 1.82$, $H_u/D = 0.85$, $H_u/L_u = 0.033$, and density = 4.4%. Within an enclosed area of 0.916 m², a total of eight spheres

of 0.08 m diameter each were placed. Simulations were carried out for four different variations in spatial distribution [Fig. 11(a)] while keeping all the other conditions the same. Similarly, in the second subset of experiments, $F_u = 1.82$, $H_u/D = 0.31$, $H_u/L_u = 0.033$, and density = 24.5%. Within an enclosed area of 1.24 m², a total of eight spheres of 0.22 m diameter each were placed. Fig. 11(b) shows the energy loss estimated by analyzing the simulated three-dimensional velocity field for the previous eight runs. It is observed from Fig. 11(b) that for a given set of flow and geometric parameters (F_u, H_u/D, H_u/L_u, and density) the energy loss did not vary significantly when the spatial distribution of the roughness elements changed. Difference in the energy loss was 7.2% when $H_u/D < 0.5$ and it was only 3% when $H_u/D > 0.5$.

Next, numerical experiments were carried out to study how the energy loss varies with cluster density, when all the other flow and geometric parameters remain the same. In the first subset of experiments, $F_u = 1.82$, $D = 8$ cm, $H_u/D = 0.85$, and $H_u/L_u = 0.033$. The density was varied from 0.7 to 16.44% by varying the number of boulders within a fixed enclosed area of 0.916 m² [Fig. 12(a)]. In the second subset of experiments, $F_u = 1.82$, $D = 22$ cm, $H_u/D = 0.31$, and $H_u/L_u = 0.033$. The density was varied from 6 to 24.5% by varying the number of boulders within a fixed enclosed area of 1.24 m². Fig. 12(b) shows the variation in energy loss with density. It is observed from Fig. 12(b) that, as expected, the energy loss increased as the number of roughness elements, i.e., density increased. However, the energy loss tended to attain an asymptotic value as the number of boulders increased beyond a point because the cluster tended to behave as one single roughness element. It is shown in Fig. 12(a) that the velocity in the
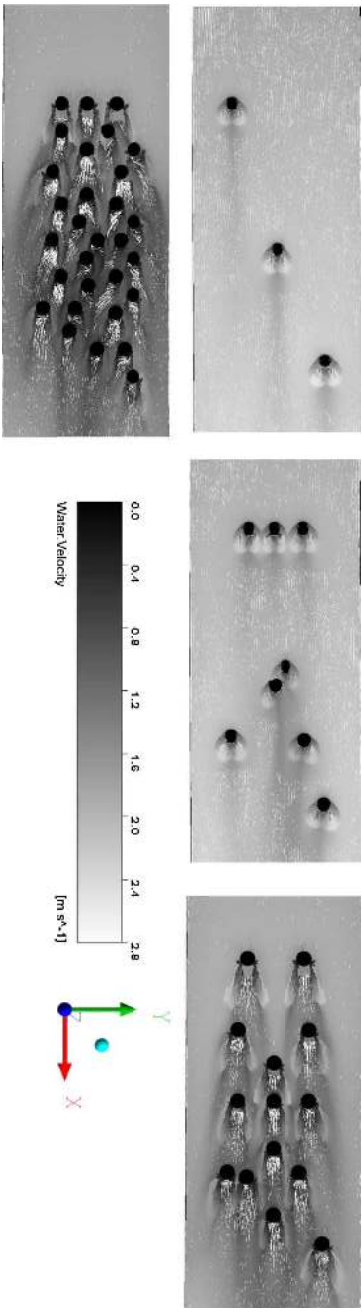
Fig. 12. Variation in energy loss with cluster density

region between the roughness elements tended to a low value as the number of boulders increased and the space between the roughness elements got diminished. A numerical run was made with a single roughness element whose size and shape was the same as the space enclosed by 30 roughness elements shown in Fig. 12(a). The energy loss for this case was 0.11 m, which is slightly higher than the asymptotic value (0.1 m) shown in Fig. 12(b).

Based on the results of the 60 numerical experiments and Eq. (6), it was possible to determine I_f values. Depending on different ranges of relative submergence, these I_f values are then used to derive the following empirical relations:

$$I_f = 0.06(\lambda)^{-0.66} F_u^{1.46} \left(\frac{H_u}{D}\right)^{-3.40} \left(\frac{H_u}{L_u}\right)^{1.10} \quad \text{for } 0.2 < \frac{H_u}{D} < 0.5 \tag{14a}$$

$$I_f = 8.20(\lambda)^{-0.36} F_u^{1.50} \left(\frac{H_u}{D}\right)^{-1.10} \left(\frac{H_u}{L_u}\right)^{1.80} \quad \text{for } 0.5 < \frac{H_u}{D} < 1.0 \tag{14b}$$

$$I_f = 2.0(\lambda)^{-0.37} F_u^{0.22} \left(\frac{H_u}{D}\right)^{-0.57} \left(\frac{H_u}{L_u}\right)^{1.00} \quad \text{for } 1.0 < \frac{H_u}{D} < 2.40 \tag{14c}$$

Comparing the empirically estimated energy loss [Eqs. (6), (13), and (14)] with the energy loss from the 60 three-dimensional

ANSYS-CFX simulations indicate the potential of the empirical approach (Fig. 13).

An attempt is made to estimate value of the total Darcy-Weisbach roughness coefficient based on the proposed model for energy loss, and compare it with the value obtained using the empirical equation proposed by Pagliara and Chiavaccini (2006). The comparison indicated an average of 85% difference in the values. This difference can be attributed to very different conditions in the experiments conducted by Pagliara and Chiavaccini (2006). Pagliara and Chiavaccini (2006) reported that the increase in energy
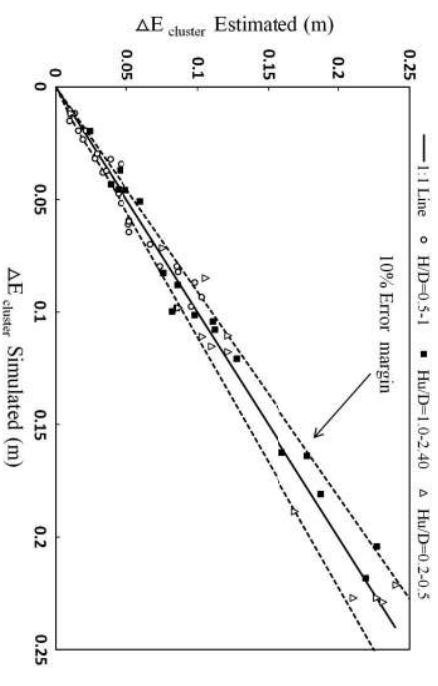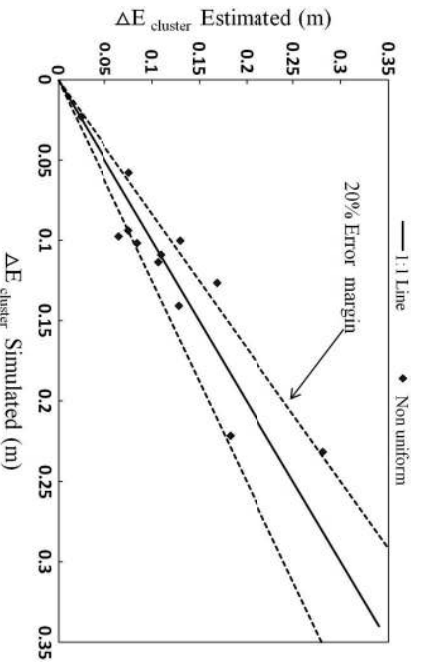

Fig. 13. Estimated and simulated energy loss for a cluster of boulders of uniform size

Fig. 14. Validation of empirical procedure for estimating energy loss due to cluster of nonuniformly sized boulders

loss due to boulders, in the tested range, depends only on disposition, roughness of boulders and the density, and not on either Froude number or relative submergence. This aspect requires further exploration.

The energy loss in the case of cluster of nonuniform sized roughness elements was estimated based on the concept of effective boulder size, D_{eff}. Validity of the proposed simple approach was tested using 12 numerical experiments (Table S3 in Supplemental Data). The ΔE for the cluster of nonuniform sized boulders calculated using the simple empirical approach is compared with the ΔE value obtained from the three-dimensional numerical simulations in Fig. 14. It is shown in Fig. 14 that the error in the estimation using the simple approach lies mostly (8 out of 12 data points) within 20% for the experiments carried out i.

The previous procedure is proposed in this study only for its simplicity, and to test to what extent simple empirical equation approach can be extended for estimating the energy loss in natural mountainous streams. In reality, the flow structure in the space between randomly distributed differently sized boulders is very complex. The interaction between the boulders depends on the approach flow conditions, sizes of neighboring boulders, and the local relative submergence value, rather than the relative submergence value based on approach flow depth. Four numerical runs (Figs. 15 and 16) were carried out to test the concept of effective size for a simple case of two boulders of unequal size. In Run 124a, two boulders of sizes $D_1 = 0.138$ m and $D_2 = 0.10$ m were kept at a distance of 0.25 m, and in Run 124b, two boulders of equal size, $D_{\mathrm{eff}} = 0.12$ m were kept a distance of 0.25 m. In both these runs (Fig. 15), the approaching flow conditions, i.e., discharge (0.45 m³/s), H_u (0.142 m), L_u (1.15 m), and S_0 were the same. It was found that energy loss due to boulders in Run 124a was 0.055 m, while it was 0.052 m in Run 124b. There was only a difference of 5.5% in the energy loss in this case when $H_u/D_{\mathrm{eff}} > 1.0$.

However, results were very different when the submergence ratio was less than 1.0. In Run 125a, two boulders of sizes $D_1 = 0.138$ m, and $D_2 = 0.10$ m were kept at a distance of 0.25 m and in Run 125b, two boulders of equal size, $D_{\mathrm{eff}} = 0.12$ m were kept a distance of 0.25 m. In both these runs (Fig. 16), the approaching flow conditions, i.e., discharge (0.1 m³/s), H_u (0.069 m), L_u (1.15 m), and S_0 were the same. It was found that energy loss in Run 125a was 0.024 m, whereas it was 0.03 m in Run 125b. There was a significant difference of 20% in this case where $H_u/D_{\mathrm{eff}} < 1.0$. Further research is needed to improve the accuracy of empirical approach by introducing a parameter which represents not only the effect of size distribution of boulders but distribution of relative submergence.

Conclusion

Macroroughness elements such as boulders induce significant energy loss in open channels. In this work, a three-dimensional
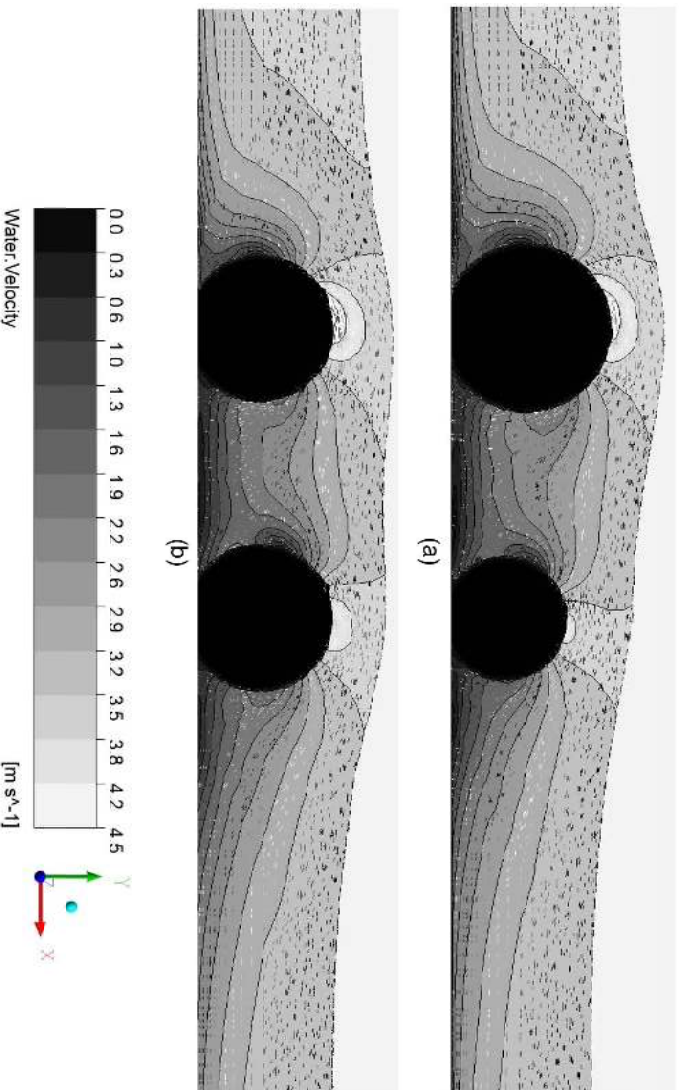
Fig. 15. Spatial variation of velocity on the central vertical plane: Run 124
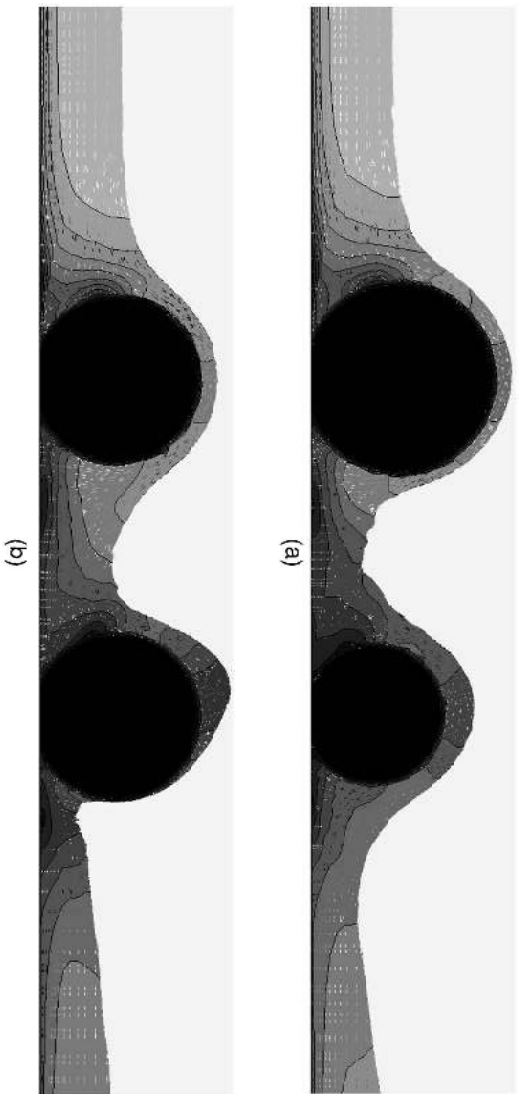
turbulent flow model was used to study the energy loss in a steeply sloping open channel induced by a single boulder and a cluster of randomly placed boulders. The three-dimensional *ANSYS-CFX* model was tested using experimental data available in literature prior to its use for performing extensive numerical experiments.

In the case of a single boulder, the energy loss could be expressed as a power function of the upstream Froude number and the relative submergence. The energy loss increases with Froude number, while it decreases with increasing relative submergence. However, the exponents in the power law relationship are different for three different ranges of relative submergence: <0.5, 0.5–1.0, and >1.0. The exponent for the Froude number ranges from 1.42 to 2.30, whereas the exponent for relative submergence varies from −0.46 to −1.77.

In the case of a cluster of boulders, for the same number of uniformly sized boulders in a cluster, the pattern of placement of boulders does not have significant effect on energy loss (<4%), especially when relative submergence is more than 0.5. Also, for the same number of boulders, the energy loss decreases as the cluster density increases. The energy loss between two sections could be expressed as a product of energy loss due to a single boulder, the number of boulders and an interaction factor. The interaction factor is a power function of (1) the upstream Froude number, (2) relative submergence, (3) cluster density, and (4) the distance between the upstream section and the cluster location. The proposed empirical procedure estimates the energy loss within a 10% error margin when the boulder size in the cluster is uniform. The error in the estimated energy loss on the basis of the concept of effective boulder size is within 20% margin if the boulder size is nonuniform.

Further research is needed for improving the predictive capability of proposed approach. Also, further investigations are needed for studying the effect of grain or bed roughness and channel slope on the energy loss due to macroroughness elements. Results from the present study are useful for estimating the energy loss in mountainous channels.

Notation

The following symbols are used in this paper:

$$4\rho V_u H_u / \mu = \mathrm{R}_u = \text{Reynolds number at the upstream section;}$$

b = width of cluster;

D = diameter of boulder or roughness element;

$D_{eff} = \sqrt{D_1^2 + D_1^2 + \cdots + D_N^2 / N}$ = effective diameter,

$D_1, D_2, \ldots, D_N$ = boulder diameters of N number of boulders;

H_u = average flow depth at upstream section;

H_u / D = relative submergence;

I_f = interaction factor;

k_s = equivalent sand grain roughness height;

L_u = location of the boulder from the upstream section;

l = length of cluster;

lb = cluster area;

N = number of boulders;

Q = flow rate;

S_o = bed slope;

TE_d = total energy at downstream section;

TE_u = total energy at upstream section;

V_u = average velocity at upstream section;

Fig. 16. Spatial variation of velocity on the central vertical plane: Run 125

$V_u / \sqrt{gH_u} = F_u$ = Froude number at upstream section;

X = length between upstream and downstream sections;

$Z = B$ = distance between sides of channel = width of channel;

ΔE_{bed} = energy loss due to bed friction;

$\Delta E = \Delta TE - \Delta E_{bed}$ = energy loss due to roughness elements;

$\Delta E^*_{single} = [\Delta E/L_u]_{single}$ = nondimensional energy loss for single boulder;

$\Delta E_{single} = [\Delta E/L]_{single}$ = energy loss single boulder;

$\Delta E^*_{cluster} = [\Delta E/L]_{cluster}$ = nondimensional energy loss for cluster of boulders;

$\Delta E_{cluster}$ = energy loss due to cluster;

ΔE_{single} = energy loss single roughness element;

ΔTE = total energy loss consist of bed friction and roughness elements; and

$\lambda = [N(\pi/4)D^2]/(Lb)$ = cluster density.

Supplemental Data

Tables S1–S3 are available online in the ASCE Library (www.ascelibrary.org).

References

Abdulla, A. A. (2013). "Three-dimensional flow model for different cross-section high-velocity channels." Ph.D. thesis, School of Marine Sciences and Engineering, Univ. of Plymouth, Plymouth, U.K.

Agostino, V. D., and Michelini, T. (2015). "On kinematics and flow velocity prediction in step-pool channels." *Water Resour. Res.*, 51(6), 4650–4667.

Aguirre-Pe, J., and Fuentes, R. (1990). "Resistance to flow in steep rough streams." *J. Hydraul. Eng.*, 10.1061/(ASCE)0733-9429(1990)116:11(1374), 1374–1387.

Alonso, R. L., Fernández, J. B., and Cugat, M. C. (2009). "Flow resistance equations for mountain rivers." *Forest Syst.*, 18(1), 81–91.

ANSYS-CFX version 14.0 [Computer software]. ANSYS, Canonsburg, PA.

Baki, A. B. M., Zhu, D. Z., and Rajaratnam, N. (2014). "Mean flow characteristics in a rock-ramp type fish pass." *J. Hydraul. Eng.*, 10.1061/(ASCE)HY1943-7900.0000816, 156–168.

Baki, A. B. M., Zhu, D. Z., and Rajaratnam, N. (2016). "Flow simulation in a rock-ramp fish pass." *J. Hydraul. Eng.*, 10.1061/(ASCE)HY1943-7900.0001166, 4016031.

Bathurst, J. C. (1985). "Flow resistance estimation in mountain rivers." *J. Hydraul. Eng.*, 10.1061/(ASCE)0733-9429(1985)111:4(625), 625–643.

Bathurst, J. C. (2002). "At-a-site variation and minimum flow resistance for mountain rivers." *J. Hydrol.*, 269(1–2), 11–26.

Bathurst, J. C., Li, R. M., and Simons, D. B. (1979). "Hydraulics of mountain rivers." *Rep. NCER78-79JCB-RML-DBS55*, Civil Engineering Dept., Colorado State Univ., Fort Collins, CO.

Bathurst, J. C., Li, R. M., and Simons, R. M. (1981). "Resistance equation for large-scale roughness." *J. Hydraul. Div.*, 107(12), 1593–1613.

Cassan, L., and Laurens, P. (2016). "Design of emergent and submerged rock-ramp fish passes." *Knowl. Manage. Aquat. Ecosyst.*, 417(10), 45.

Cassan, L., Tien, T., Couret, D., Laurens, P., and Dartus, D. (2014). "Hydraulic resistance of emergent macroroughness at large Froude numbers: Design of nature-like fishpasses." *J. Hydraul. Eng.*, 10.1061/(ASCE)HY1943-7900.0000910, 4014043.

Castillo, L. G., Carrillo, J. M., García, J. T., and Vigueras-Rodríguez, A. (2014). "Numerical simulations and laboratory measurements in hydraulic jumps." *Proc., 11th Int. Conf. on Hydroinformatics*, CUNY Academic Works, New York.

Chin, A. (2003). "The geomorphic significance of step-pools in mountain streams." *Geomorphology*, 55(1–4), 125–137.

Comiti, F., Mao, L., Wilcox, A., Wohl, E. E., and Lenzi, M. A. (2007). "Field-derived relationships for flow velocity and resistance in high-gradient streams." *J. Hydrol.*, 340(1–2), 48–62.

Evans, M. W., Harlow, F. H., and Bromberg, E. (1957). "The particle-in-cell method for hydrodynamic calculations." *Technical Rep., DTIC Document*, Lol Alamos Scientific Laboratory, Los Alamos.

Ferguson, R. (2007). "Flow resistance equations for gravel- and boulder-bed streams." *Water Resour. Res.*, 43(5), 1–12.

Ferguson, R. (2010). "Time to abandon the Manning equation?" *Earth Surf. Processes Landforms*, 35(15), 1873–1876.

Ferro, V. (2003). "Flow resistance in gravel-bed channels with large-scale roughness." *Earth Surf. Processes Landforms*, 28(12), 1325–1339.

Haltigin, T. W., Biron, P. M., and Lapointe, M. F. (2007). "Three-dimensional numerical simulation of flow around stream deflectors: The effect of obstruction angle and length." *J. Hydraul. Res.*, 45(2), 227–238.

Hey, R. D. (1979). "Flow resistance in gravel-bed rivers." *J. Hydraul. Div.*, 105(4), 365–379.

Hirt, C. W., and Nichols, B. D. (1981). "Volume of fluid (VOF) method for the dynamics of free boundaries." *J. Comput. Phys.*, 39(1), 201–225.

Jones, W. P., and Launder, B. E. (1972). "The prediction of laminarization with a two-equation model of turbulence." *Int. J. Heat Mass Transfer*, 15(2), 301–314.

Jordanova, A. A. (2008). "Low flow hydraulics in rivers for environmental applications in South Africa." Ph.D. dissertation, Univ. of Witwatersrand, Johannesburg, South Africa.

Ma, L., Ashorth, P. I., Best, J. L., Elliott, L., Ingham, D. B., and Whitcombe, L. J. (2002). "Computational fluid dynamics and the physical modelling of an upland river." *Geomorphology*, 44(3), 375–391.

Maloney, K. O., Munguia, P., and Mitchell, R. M. (2011). "Anthropogenic disturbance and landscape patterns affect diversity patterns of aquatic benthic macroinvertebrates." *J. North Am. Benthol. Soc.*, 30(1), 284–295.

Marriner, B. A., Baki, A. B. M., Zhu, D. Z., Thiem, J. D., Cooke, S. J., and Katopodis, C. (2014). "Field and numerical assessment of turning pool hydraulics in a vertical slot fishway." *Ecol. Eng.*, 63, 88–101.

Marriott, M. J., and Jayaratne, R. (2010). "Hydraulic roughness—Links between Manning's coefficient, Nikuradse's equivalent sand roughness and bed grain size." *Advances in computing and technology*, Univ. of East London, London, 27–32.

Meier, W. K., and Reichert, P. (2005). "Mountain streams—Modeling hydraulics and substance transport." *J. Environ. Eng.*, 10.1061/(ASCE)0733-9372(2005)131:2(252), 252–261.

Modrick, T. M., and Georgakakos, K. P. (2014). "Regional bankfull geometry relationships for southern California mountain streams and hydrologic applications." *Geomorphology*, 221, 242–260.

Oertel, M., Peterseim, S., and Schlenkhoff, A. (2011). "Drag coefficients of boulders on a block ramp due to interaction processes." *J. Hydraul. Eng.*, 49(3), 372–377.

Pagliara, S., and Chiavaccini, P. (2006). "Flow resistance of rock chutes with protruding boulders." *J. Hydraul. Eng.*, 10.1061/(ASCE)0733-9429(2006)132:6(545), 545–552.

Pagliara, S., and Dazzini, D. (2002). "Hydraulics of block ramp for riverrestoration." *Proc., New Trends in Water and Environmental Engineering for Safety and Life: Eco-Compatible Solution for Aquatic Environments*, Capri, CSDU, Milano, Italy.

Pagliara, S., and Peruginelli, A. (2000). "Energy dissipation comparison among stepped channel, drop and ramp structures." *Proc., Workshop on Hydraulics of Stepped Spillways*, A.A. Balkema, Rotterdam, Netherlands, 111–118.

Romero, M., Revollo, N., and Molina, J. (2010). "Flow resistance in steep mountain rivers in Bolivia." *J. Hydrodyn.*, 22(5), 702–707.

Salaheldin, T. M., Imran, J., and Chaudhry, M. H. (2004). "Numerical modeling of three-dimensional flow field around circular piers." *J. Hydraul. Eng.*, 10.1061/(ASCE)0733-9429(2004)130:2(91), 91–100.

Shen, Y., and Diplas, P. (2008). "Application of two- and three-dimensional computational fluid dynamics models to complex ecological stream flows." *J. Hydrol.*, 348(1–2), 195–214.

Soto, A. U., and Madrid-Aris, M. (1994). *Roughness coefficient in mountain rivers*, ASCE, New York, 1–8.

Thompson, S. M., and Campbell, P. L. (1979). "Hydraulics of a large channel paved with boulders." *J. Hydraul. Res.*, 17(4), 341–354.

Thorne, C. R., and Zevenbergen, L. W. (1985). "Estimating mean velocity in mountain rivers." *J. Hydraul. Eng.*, 10.1061/(ASCE)0733-9429 (1985)111:4(612), 612–624.

Xiang, M., Cheung, S. C. P., Tu, J. Y., and Zhang, W. H. (2014). "A multi-fluid modelling approach for the air entrainment and internal bubbly flow region in hydraulic jumps." *Ocean Eng.*, 91, 51–63.

Yochum, S. E., Bledsoe, P. B., David, G. C. L., and Wohl, E. (2012). "Velocity prediction in high gradient channels." *J. Hydrol.*, 424, 84–98.